Theoretical investigation of the instrumental peak line shape in ion-scattering spectroscopy

Vaneica Y. Young and Nicole Welcome
Department of Chemistry, University of Florida, Gainesville, Florida 32611-2046

Gar B. Hoflund
Department of Chemical Engineering, University of Florida, Gainesville, Florida 32611-2023
(Received 29 June 1992; revised manuscript received 1 February 1993)

The instrumental peak line shape describing the elastic scattering of a single isotopic primary ion off a single isotopic target surface has been investigated theoretically using a Bohr-screened Coulomb potential, the Thomas-Fermi-Firsov-screened Coulomb potential, and the Ziegler-Biersack-Littmark universal potential. Experimental factors such as the energy spread in the primary ion beam and the spectral resolution (channel width) have also been taken into account in this study. The calculated line shapes have been determined for 100 eV ^{4}He scattering off ^{27}Al and ^{193}Nb with a scattering angle $\theta = 143°$ and a $\Delta\theta$ of $\pm 12°$. The results show that the ion-scattering spectroscopy peaks are asymmetrical due to the variation in differential scattering cross section with energy. This asymmetry is more pronounced for Al (lighter mass), higher spectral resolution, and narrower primary ion energy distributions.

I. INTRODUCTION

Apparently, Nelson[1] was the first to propose a model for the decomposition of ion-scattering spectra. In this model the peak due to elastically scattered ions is represented by a combined Gaussian and Lorentzian function, which has a symmetrical peak line shape. However, experimental ion-scattering spectroscopy (ISS) peak shapes are often asymmetrical. In order to gain an understanding of this asymmetry, many different processes have been considered and examined. The presence of isotopes in either the primary ion beam or the target can result in asymmetry of the ISS peaks.[2–4] Other processes which can contribute to peak asymmetry include neutralization-reionization, multiple scattering, and target-atom vibration.[5] In the absence of these processes, the underlying assumption has usually been made that a symmetrical peak is obtained when a single isotopic primary ion scatters off of a single isotopic target.

A decompositional approach for the analysis of ISS data is useful because it can be applied as a tool for obtaining the composition of the outermost atomic layer of a surface quantitatively. The other approach for the theoretical investigation of ion-scattering spectra is by means of simulation. In this type of study, physical processes which may affect a projectile interacting with a multilayer target are included in a model. Then the energy distribution of the backscattered projectiles is calculated. The background, which consists of multiple scattered projectiles, is implicitly determined in this calculation. More complex models also allow for the determination of the angular distribution of the backscattered projectiles. Three types of simulation have been employed: Monte Carlo simulation based on the binary collision approximation, molecular dynamics simulation, and simulation using transport theory. Hou[6] has reviewed the former two types of simulations thoroughly. The Monte Carlo approach is based on following the trajectory of a projectile and recording its energy losses until it leaves the target surface or is trapped within the target. This process is repeated for a large number of projectiles, which yields a histogram approximating the ion-scattering spectrum. In molecular dynamics the motion of a collection of particles is followed as a function of time. Their motion is governed by an interatomic pairwise potential and determined by numerical integration of the Hamiltonian equations. Simulation using transport theory involves calculation of the projectile reflection coefficient, which is related to the projectile range distribution through an integral equation.[7] Simulation is an excellent research tool for examining the importance of various physical processes in ISS. Although the results of simulation studies can assist in the development of effective computer codes for spectral decomposition, simulation methods are too complex for routine analytical quantification.

As discussed below, the instrumental peak line shape results from a convolution of factors, and one of these factors is the differential scattering cross section. In order to calculate differential scattering cross sections, an interaction potential between the collision partners must be selected. Differential cross sections calculated using the Born-Mayer potential[8] increase with primary ion energy and decrease with scattering angle. For this potential function, ISS peak line shapes are asymmetric if these two opposing effects do not exactly cancel. The Born-Mayer potential[9] has the mathematical form

$$V(r) = A \exp(-br) , \tag{1}$$

where r is the relative position between the collision partners and A and b are model parameters obtained by least-squares fitting of the linear region observed for the Thomas-Fermi-Dirac (TFD) potential. This is an approximate potential with a domain $[r_1, r_2]$ which is typically $[1.5\ a_0, 3.5\ a_0]$, where a_0 is the Bohr radius of the

hydrogen atom. Since the turning point for ISS does not lie within this domain, this potential is not expected to yield cross sections which are adequate for quantitative ISS studies. No such limitation applies to the TFD potential itself,[10] which is given by

$$U_0(r)=\frac{Z_1Z_2e^2}{r}+H_0-H_0(\infty)\ , \tag{2}$$

where $H_0-H_0(\infty)$ is the total electron energy of the collision partners relative to the total electron energy at infinite separation and Z_1 and Z_2 are the atomic numbers of the collision partners. $U_0(r)$ cannot be evaluated analytically so it is approximated by the average potential[10]

$$\overline{U}(r)=\frac{Z_1Z_2e^2}{r}S\left[\frac{r}{a}\right]-\frac{k_\alpha^2}{120K_\kappa}(Z_1+Z_2)+\overline{\Lambda}\ , \tag{3}$$

where $S(r/a)$ is a screening function, k_α and K_κ are constants, and $\overline{\Lambda}$ is a linear combination of integrals involving the electron density. This latter term limits the application of this potential function because it is difficult to evaluate the integrals. Only a quantum-mechanical interaction potential, which allows the effect of electron shells to be treated, gives a better description of the scattering process. If electron exchange is neglected in Eq. (3), then the Thomas-Fermi potential is obtained:

$$V(r)=\frac{Z_1Z_2e^2}{r}S\left[\frac{r}{a}\right]\ . \tag{4}$$

The various forms of the Thomas-Fermi potential differ in the form of the screening function. The Thomas-Fermi-Firsov screening function[11] is given by

$$S(r/a)=\theta[(Z_1^{1/2}+Z_2^{1/2})^{2/3}r/0.468]\ , \tag{5}$$

where θ is the dimensionless Thomas-Fermi function given by

$$\theta(x)=\frac{r}{Ze}[V(r)-V_0]\ , \tag{6}$$

where x is the dimensionless variable $x=r/\mu$, with μ the screening length; $\mu=0.8853\ a_0/Z^{1/3}$. This function must satisfy the Thomas-Fermi equation,

$$\theta''(x)=\theta(x)^{3/2}/x^{1/2}\ . \tag{7}$$

Furthermore, $\theta(x)$ depends on the electron density,

$$\rho(r)=\frac{Z}{4\pi\mu^3}\left[\frac{\theta(x)}{x}\right]^{3/2}=\frac{Z}{4\pi\mu^3}\frac{\theta''(x)}{x}\ . \tag{8}$$

The Thomas-Fermi-Moliere screening function[12] is given by

$$S(r/a)=0.1\exp(-6[r/a])+0.55\exp(-2[r/a])+0.35\exp(-0.3[r/a])\ , \tag{9}$$

where a is given by

$$a=0.468C(Z_1^{2/3}+Z_2^{2/3})^{-1/2}\ , \tag{10}$$

and C is an empirically derived constant. In this case the Thomas-Fermi function θ is approximated by a linear combination of exponential functions in order to simplify the calculations.

The simplest way of treating electron interaction effects is to multiply the Coulomb potential by a damping function. Classically, the Bohr screening function[13] is often used. It has the form

$$S(r/a)=\exp(-r/a)\ , \tag{11}$$

with

$$a=a_0(Z_1^{2/3}+Z_2^{2/3})^{-1/2}\ . \tag{12}$$

A comparison of the Bohr screening function with the Moliere screening function shows that it is a fair approximation to the Thomas-Fermi function even though it does not formally consider electron-nuclei and electron-electron interactions. According to Miller,[5] differential cross sections calculated using these three screening functions give curves which are qualitatively similar to those derived using the Born-Mayer potential.

The above discussion suggests that the assumption that a symmetrical peak is obtained when a single isotopic primary ion scatters off of a single isotopic target may be invalid. The Thomas-Fermi-Moliere-screened potential has been widely used in ion-scattering studies. It was not used in this study because the constant C must be derived empirically and adjusted to give the best fit between theory and experiment. Therefore, different values are obtained for different primary-target pairs. No empirical parameters are required to evaluate the TFFSC or the BSC potentials. Furthermore, Parilis[14] has shown that the Thomas-Fermi-Firsov-screened Coulomb (TFFSC) potential gives results which are in good agreement with experiment for primary ion energies greater than 1000 eV. Of the classical potentials the BSC potential is the most frequency used. It is valid for scattering angles greater than a few degrees and for primary ion energies ranging from 100 to hundreds of thousands of eV.[13] More recently, Ziegler, Biersack, and Littmark (ZBL)[15] have developed a universal potential which is superior to the three potentials discussed above. The ZBL potential accounts for the effect of the electron shell structures of the collision partners. The screening function for the ZBL potential is given by

$$\begin{aligned}S(r/a)=&0.1818\exp(-3.2[r/a])\\&+0.5099\exp(-0.9423[r/a])\\&+0.2802\exp(-0.4028[r/a])\\&+0.02817\exp(-0.2016[r/a])\ ,\end{aligned} \tag{13}$$

where

$$a=\frac{0.8858a_0}{Z_1^{0.23}+Z_2^{0.23}}\ . \tag{14}$$

Apparently, the ZBL potential has not been used to calculate ISS cross sections even though cross sections calculated using this potential should be better than those calculated using the TFFSC or BCS potentials. Therefore, the TFFSC, BSC, and ZBL potential functions have been used in this study to investigate ISS line shapes.

Three experimental parameters; the spread in the energy of the primary ion beam, the acceptance aperture of the analyzer, and the spectral resolution (channel width), have been taken into account in these calculations. Two target materials; Al and Nb, have been selected because they each consist of only one naturally occurring isotope and have very different masses.

II. THEORETICAL MODEL

Ideally, the normalized spectral peak for scattering of $^4He^+$ off Nb would be described by the function

$$P(E_s)=\begin{cases}1 & \text{for } E_s=856.6 \text{ eV},\\ 0 & \text{otherwise},\end{cases} \tag{15}$$

assuming that the scattering obeys the binary elastic-scattering collision model for which

$$\frac{E_s}{E_p}=\left[\frac{M_p}{M_p+M_t}\right]^2\left\{\cos\theta\pm\left[\left[\frac{M_t}{M_p}\right]^2-\sin^2\theta\right]^{1/2}\right\}^2, \tag{16}$$

where E_s is the scattered energy of the primary ion, E_p is the initial energy of the primary ion, M_t is the mass of the target, M_p is the mass of the primary ion, and θ is the scattering angle referenced to the laboratory coordinate system. For $M_t>M_p$ only the positive sign applies. However, in practice an ISS peak is broadened by a number of experimental factors such as the energy distribution of the primary ion beam and the width of the acceptance window about the nominal scattering angle. These factors have been discussed quantitatively by Young, Hoflund, and Miller.[3] Ion sources used for ISS produce fluxes which have Gaussian energy distributions about the nominal energy E_p. The full width at half maximum (FWHM) of this distribution is usually expressed as some percentage of E_p, and this percentage depends on the type of ion source and the instrumental settings used. Therefore, the distribution is represented by

$$G(E;E_p,\sigma_E^2)=\frac{1}{\sigma_E\sqrt{2\pi}}\exp\left[\frac{(E-E_p)^2}{2\sigma_E^2}\right], \tag{17}$$

where E is the kinetic energy of the primary ion and σ_E^2 is the absolute variance. The scattering angle can assume values over the interval $[\theta_s-d\theta,\theta_s+d\theta]$, where θ_s is the instrumental setting for the scattering angle (143° in this study) and $2d\theta$ is the acceptance window width. Since the width is fairly small, a uniform distribution has been assumed for these calculations. It is represented by

$$T(\theta)=\begin{cases}\dfrac{1}{2d\theta} & \text{for } \theta_s-d\theta\le\theta\le\theta_s+d\theta,\\ 0 & \text{otherwise.}\end{cases} \tag{18}$$

Thus, each Cartesian pair (E,θ) yields a peak with scattered-ion energy E_s and intensity given by the convolution of $T(\theta),G(E;E_p,\sigma_E^2)$, and the differential scattering cross section. Since these three factors are independent, the differential cross section at θ does not depend on the angular distribution or the ion energy distribution. Therefore, the intensity for a given (E,θ) pair satisfies the relation

$$I(E_s,E,\theta)\propto\frac{1}{2d\theta}G(E;E_p,\sigma_E^2)\frac{d\sigma(\theta)}{d\Omega}, \tag{19}$$

where $d\sigma(\theta)/d\Omega$ is the differential scattering cross section defined by

$$\frac{d\sigma(\theta)}{d\Omega}=\frac{b}{\sin\theta}\left|\frac{db}{d\theta}\right|, \tag{20}$$

where b is the impact parameter, θ is the laboratory scattering angle, and Ω is the solid angle into which the ions scatter. The scattering angle in the center-of-mass system $\theta_{\text{c.m.}}$ depends upon the impact parameter b, the potential acting between the primary ion and the target $V(r)$, and the primary ion energy E_p according to

$$\theta_{\text{c.m.}}=\pi-2b\int_{r_m}^{\infty}\frac{dr}{r^2\left[1-\dfrac{b^2}{r^2}-\dfrac{V(r)}{E_p}\right]^{1/2}}, \tag{21}$$

where r_m is the distance of closest approach given by

$$r_m=\frac{b}{[1-V(r_m)/E_p]^{1/2}}. \tag{22}$$

Furthermore, the relationship between the laboratory scattering angle θ and the scattering angle in the center-of-mass system is given by

$$\theta_{\text{c.m.}}=\theta+\sin^{-1}\left[\left[\frac{M_p}{M_t}\right]\sin\theta\right]. \tag{23}$$

The differential scattering cross section in the center-of-mass system is given by Eq. (20) with θ replaced by $\theta_{\text{c.m.}}$ so the differential scattering cross section in the laboratory system is related to that in the center-of-mass system by[16]

$$\frac{d\sigma(\theta)}{d\Omega}=\frac{[1+(2M_p/M_t)\cos\theta_{\text{c.m.}}+(M_p/M_t)^2]^{3/2}}{1+(M_p/M_t)\cos\theta_{\text{c.m.}}}\frac{d\sigma(\theta_{\text{c.m.}})}{d\Omega}. \tag{24}$$

In this study ISS line shapes have been calculated for the scattering of 1000 eV $^4He^+$ off ^{27}Al and ^{93}Nb at a scattering angle θ of 143° and a scattering angle width $\Delta\theta$ of 12°. The calculations have been made using two different primary beam energy distributions with FWHM's of 5 and 50 eV and channel widths ranging from 0.1 to 3.0 eV. These parameters and the potential-energy function used are specified for each line shape shown in the figures.

For the BSC potential or the ZBL potential, it is not possible to obtain an analytic expression for b, but the integral in Eq. (21) can be evaluated numerically.[13] Therefore, a computer program has been written to evaluate b. Using Eq. (23), θ is converted to the center-of-mass scattering angle. Then seed values for b and r_m are taken from Table I of Ref. 13, which has been electronically filed on the same disk as the program. Values for the integrand in Eq. (21) are calculated for 1001 points over the range from r_m to $100r_m$ since a trial and error calculation showed that this function is very close to zero at $100r_m$. The integral is evaluated by taking the average of the upper and lower Riemann sums, and a new value of b is calculated using Eq. (21). The new value is compared with the old, and if

$$\left|\frac{(b_{i+1}-b_i)}{b_i}\right| > 0.001 \tag{25}$$

(more than 0.1% error), a new value for r_m is obtained by finding the largest positive root of the radical term in the denominator of the integrand function. Iteration is continued in this manner until two successive values of b have a relative error $\leq 0.1\%$. The whole procedure is completed for values of $\theta_{\text{c.m.}}$ slightly smaller and slightly larger than the scattering angle in order to obtain the derivative $db/d\theta$ by a finite difference method. Then $d\sigma(\theta_{\text{c.m.}})/d\Omega$ is evaluated using Eq. (20) with $\theta=\theta_{\text{c.m.}}$. Finally, the differential cross section is converted to the laboratory system by means of Eq. (24).

Differential cross sections based on the TFFSC potential were calculated using the equation of Parilis[14]

$$\frac{d(\theta)}{d\Omega} = 13.68\frac{\pi^2(M_p+M_t)a^2Z_pZ_t(\pi-\theta_{\text{c.m.}})}{M_t(Z_p^{1/2}+Z_t^{1/2})^{2/3}E(2\pi-\theta_{\text{c.m.}})^2\theta_{\text{c.m.}}^2\sin\theta_{\text{c.m.}}}, \tag{26}$$

where $a=0.468$ Å. Using step sizes of 1 eV and 1°, E_s and $I(E_s,E,\theta)$ were calculated for 525 Cartesian pairs (E,θ) over the energy range from 990 to 1010 eV for $\sigma_E=5$ eV and the scattering angle range from 131° to 155°. An energy range of 900 to 1100 eV with a step size of 10 eV was used for $\sigma_E=50$ eV. From the 525 pairs (E_s,I), a histogram was generated using equally spaced intervals for E_s. The size of the interval corresponds to the channel resolution. The intensity on the interval is the sum of the intensities of the points falling on the interval.

ISS spectra are usually collected digitally using a computer-interfaced pulse counter.[17] Thus, an important experimental parameter is the channel resolution, which is defined as the energy interval for a single channel. If a spectrum has an energy range of 1000 eV and is collected in 1000 channels, then the energy resolution is 1 eV.

III. RESULTS AND DISCUSSION

ISS spectra for $^4He^+$ scattering off ^{93}Nb calculated using the TFFSC potential at a resolution of 0.2 eV and a primary ion FWHM of 5 eV are shown in Fig. 1(a) and 1(b). Two starting energy values of 838.0 and 838.1 eV (a and b, respectively) were used to demonstrate that the results are not biased by how the interval is chosen. Two effects are apparent: (a) the intensities oscillate from point to point and (b) the distribution is asymmetric on the high scattering-energy side. The same effects are also apparent when the BSC potential and the ZBL potential are used to calculate the comparable spectra shown in Figs. 1(c) and 1(d). The oscillations may be a consequence of the fact that the Cartesian pairs used are integer pairs while in reality both E and θ are continuously varying functions. Experimental factors tend to smooth

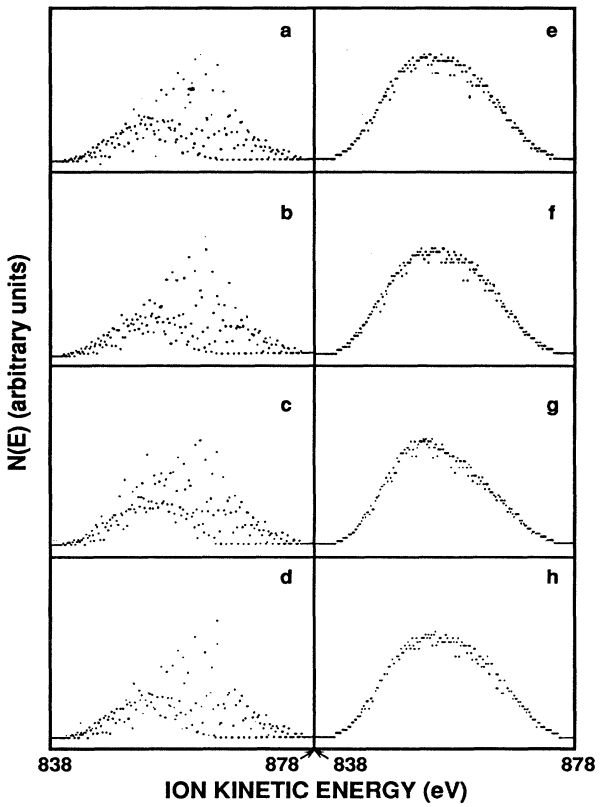

FIG. 1. Calculated ISS spectra for 1000 eV $^4He^+$ scattering off ^{93}Nb; $\theta=143°$ and $\Delta\theta=12°$, FWHM of the primary ion beam energy distribution of 5 eV and a channel width of 0.2 eV, (a) starting energy =838.0 eV, TFFSC potential, (b) starting energy =838.1 eV, TFFSC potential, (c) starting energy = 838.0 eV, BSC potential, and (d) starting energy = 838.0 eV, ZBL potential. (e), (f), (g), and (h) are the same spectra as shown in (a), (b), (c), and (d), respectively, after smoothing using a seven-point moving average.

out data, and then the data are usually smoothed further using some numerical routine. These processes would make the oscillatory nature of ISS spectra less obvious so it is reasonable to smooth the calculated spectra obtained in this study. Trial and error showed that a seven-point moving average smooth gives the best results. The smoothed spectra corresponding to those shown in Figs. 1(a)–1(d) are shown in Figs. 1(e)–1(h), respectively. Now a significant difference is observed between the spectra obtained using the three potentials. The spectrum obtained using the BSC potential is less symmetrical than the other two.

The differential cross sections calculated using the TFFSC potential and the ZBL potential decrease uniformly with increasing scattering angle for fixed scattered-ion energy. As shown in Fig. 2, the differential cross sections calculated using the BSC potential do not decrease uniformly for the same conditions. About 3% of the calculated points have large values, which result in spikes in the calculated histogram, but the spikes are reduced by averaging. These large values do not occur at the same value of θ or in any predictable manner and are not observed for all values of E over the range of θ examined. Everhart, Stone, and Carbone[13] report that this occurs when the second term in Eq. (21) is close to π. There does not appear to be a physical basis for these oscillations. Everhart, Stone, and Carbone[13] also show plots of the differential scattering cross sections which decrease as the angle increases. Unfortunately, the plots terminate at $\theta = 108°$. In Table I of that same paper, tabulated values of the differential scattering cross section are given for $\theta = 1.8°$, 3.6°, 5.4°, 7.2°, 10.8°, 14.4°, 18°, 27°,

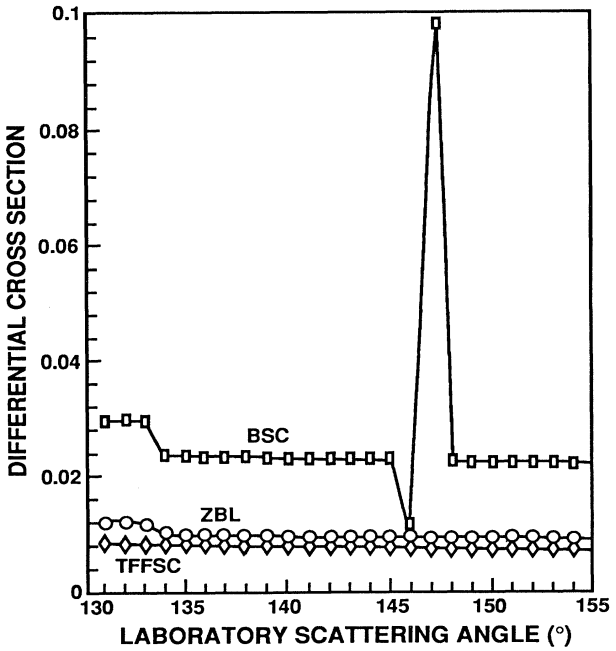

FIG. 2. Comparison of the differential scattering cross sections (in Å^2/sr) calculated using the BSC, TFFSC, and ZBL potentials for $E_p = 1000$ eV.

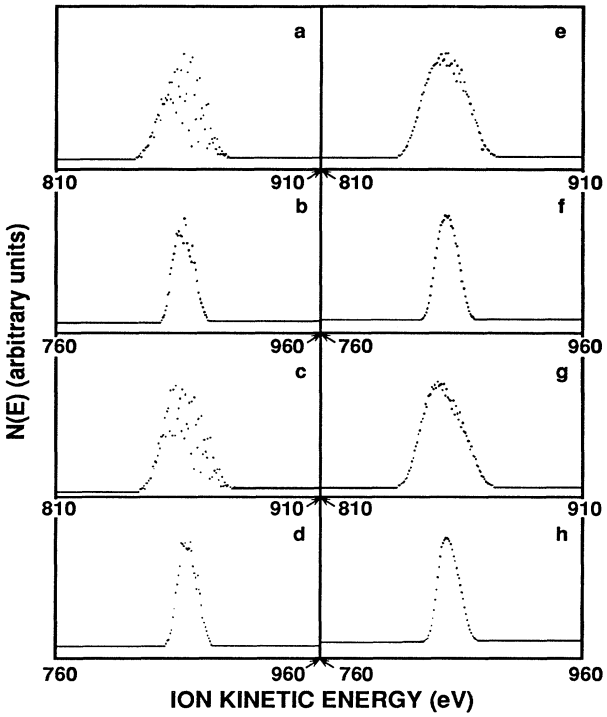

FIG. 3. Calculated ISS spectra for 1000 eV $^4He^+$ scattering off ^{93}Nb using a 5 eV FWHM primary ion bean and (a) TFFSC potential and a channel width of 0.5 eV, (b) TFFSC potential and a channel width of 1.0 eV, (c) BSC potential and a channel width of 0.5 eV, (d) BSC potential and a channel width of 1.0 eV. (e), (f), (g), and (h) are seven-point moving average smoothed curves corresponding to (a), (b), (c), and (d), respectively.

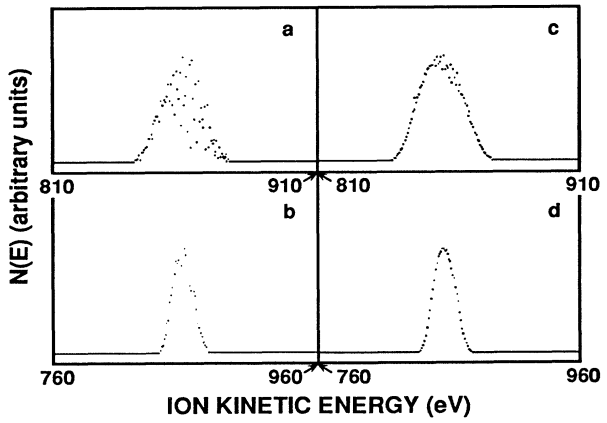

FIG. 4. Calculated ISS spectra for 1000 eV $^4He^+$ scattering off ^{93}Nb using a 5 eV FWHM primary ion beam and the ZBL potential for (a) a channel width of 0.5 eV and (b) a channel width of 1.0 eV. (c) and (d) are seven-point moving average smoothed curves corresponding to (a) and (b), respectively.

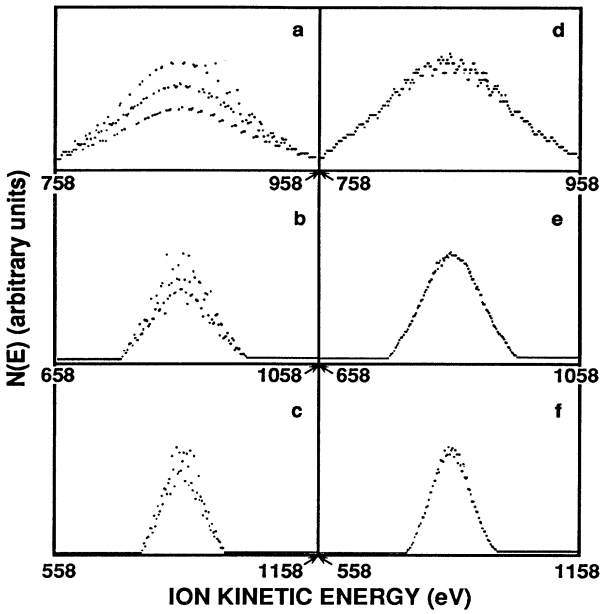

FIG. 5. Calculated ISS spectra for 1000 eV $^4He^+$ scattering off ^{93}Nb using the TFFSC potential, a 50 eV FWHM primary ion beam, and (a) a 1.0 eV channel width, (b) a 2.0 eV channel width, and (c) a 3.0 eV channel width. (d), (e), and (f) are smoothed curves corresponding to (a), (b), and (c), respectively.

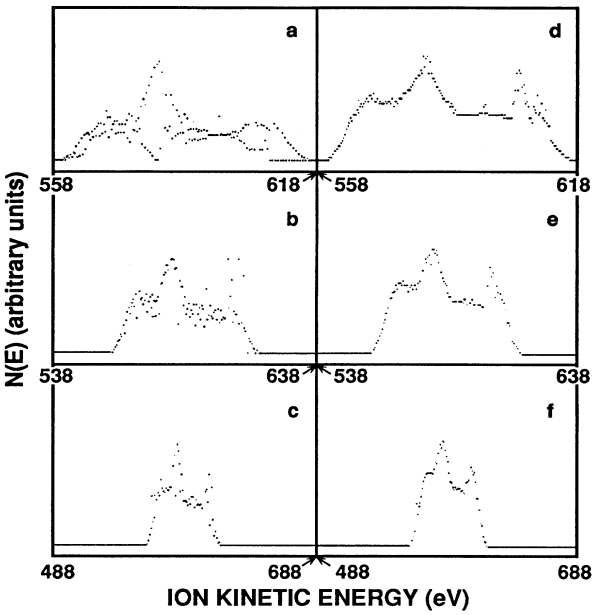

FIG. 7. Calculated ISS spectra for 1000 eV $^4He^+$ scattering off ^{27}Al using the ZBL potential, a 5 eV FWHM primary ion beam, and (a) a 0.3 eV channel width, (b) a 0.5 eV channel width, and (c) a 1.0 eV channel width. (d), (e), and (f) are smoothed curves corresponding to (a), (b), and (c), respectively.

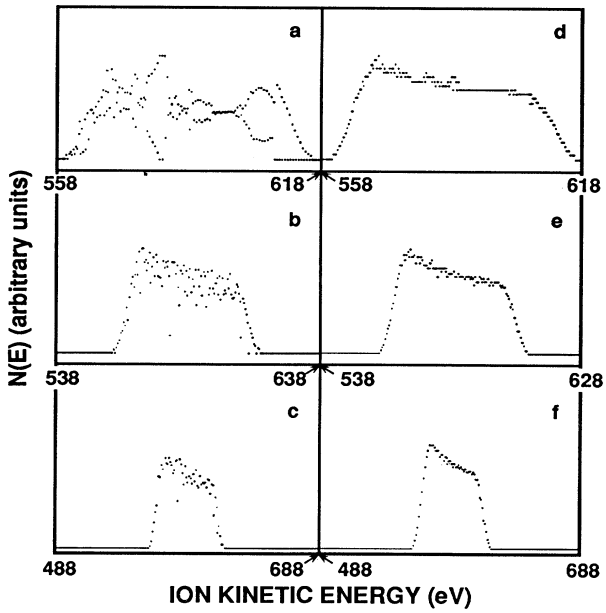

FIG. 6. Calculated ISS spectra for 1000 eV $^4He^+$ scattering off ^{27}Al using the TFFSC potential, a 5 eV FWHM primary ion beam, and (a) a 0.3 eV channel width, (b) a 0.5 eV channel width, and (c) a 1.0 eV channel width. (d), (e), and (f) are smoothed curves corresponding to (a), (b), and (c), respectively.

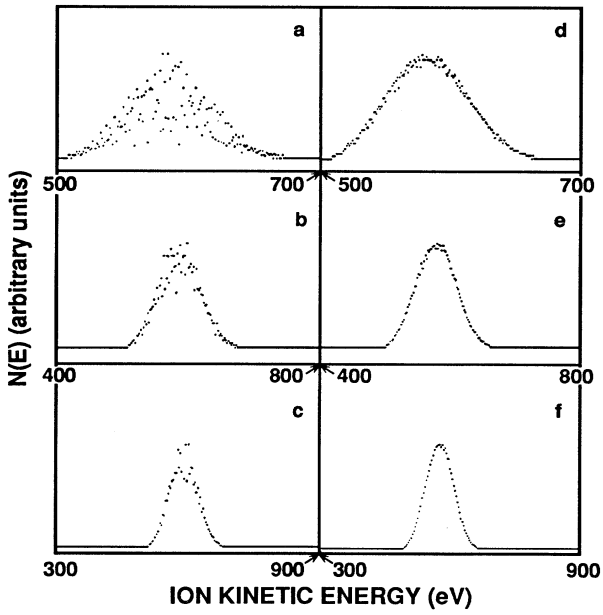

FIG. 8. Calculated ISS spectra for 1000 eV $^4He^+$ scattering off ^{27}Al using the TFFSC potential, a 50 eV FWHM primary ion beam, and (a) a 1.0 eV channel width, (b) a 2.0 eV channel width, and (c) a 3.0 eV channel width. (d), (e), and (f) are smoothed curves corresponding to (a), (b), and (c), respectively.

36°, 54°, 72°, 90°, 135°, and 180°. It is not evident how the values for $\theta=180°$ are derived. For $\theta=180°, \theta_{c.m.}$ is also 180°. Since the integral in Eq. (21) is not zero, b must be zero, which makes sense in order to get 180° backscattering. Thus, according to Eq. (20), the differential cross section becomes undefined. It is likely that the authors used graphical linearization to obtain the value for 180°. Although the same computer algorithm has been used for both the BSC and ZBL calculations, the results obtained using the ZBL potential do not exhibit oscillations. Further studies are necessary to develop a better understanding of the variations of the scattering parameters with angle. However, the important observation is that ISS peak asymmetry is predicted using all three potential-energy functions.

Spectra calculated using the three potential-energy functions at lower spectral resolutions of 0.5 and 1.0 eV are shown in Figs. 3 and 4 along with the corresponding seven-point smoothed spectra. Generally, the peak shapes become more symmetrical as the spectral resolution decreases. Asymmetry is still observed in all four smoothed spectra, but it is less apparent for the spectra calculated using the TFFSC potential or the ZBL potential.

ISS spectra are shown in Fig. 5 which were calculated at even lower resolution than those in Figs. 1, 3, and 4. They were calculated using the TFFSC potential, a FWHM=50 eV for the primary ion beam and channel widths of 1.0, 2.0, and 3.0 eV. As expected, the calculated spectra become more symmetrical as the experimental resolution decreases. The lowest resolution smoothed spectrum shown in Fig. 5(f) appears to be quite symmetrical.

Similar calculations have also been carried out for 1000 eV $^4He^+$ scattering off ^{27}Al at $\theta=143°$, $\Delta\theta=\pm12°$, and $\sigma_E=5$ eV using the TFFSC potential and the ZBL potential. This has been done because lower mass targets inherently have higher resolution in ISS than higher mass targets. Both the raw and seven-point smoothed spectra are shown in Figs. 6 and 7. The spectra calculated using the TFFSC potential and the ZBL potential are quite different. The differential cross section calculated using the ZBL potential decreases uniformly with increasing scattering angle for scattering off ^{93}Nb, but the differential cross section for $\theta=144°$ is always four to five times larger than expected. Both the raw and smoothed spectra are clearly asymmetric. At a channel resolution of 1.0 eV, the spectra would be interpreted as containing more than one peak. The peaks shown in Fig. 8 were calculated in the same manner as those in Figs. 6 and 7, but a value of $\sigma_E=50$ eV was used. Clearly, the primary beam energy distribution has a large influence on line shape indicating that nearly monoenergetic beam sources are required to obtain more accurate line shapes. The smoothed Al peak calculated at the lowest resolution considered in this study is shown in Fig. 8(f). Even for such a low-mass element, it exhibits essentially no asymmetry.

IV. CONCLUSION

ISS peak line shapes have been calculated for 1000 eV $^4He^+$ scattering off ^{27}Al and ^{93}Nb at a scattering angle $\theta=143°$ and a width $\Delta\theta=\pm12°$. The calculations have been made using the TFFSC, BSC, and ZBL potentials with varying spectral resolution (channel width) and primary ion beam energy distribution. At higher resolutions the ISS peaks obtained from Al and Nb using all three potentials are asymmetrical, but the peaks become more symmetrical as the resolution decreases. This explains why most experimental ISS peaks appear to be symmetrical.

ACKNOWLEDGMENTS

The authors appreciate the financial support received from the National Science Foundation through Grant No. CTS-9122575.

[1]G. C. Nelson, J. Vac. Sci. Technol. A **2**, 1567 (1986).
[2]V. Y. Young and G. B. Hoflund, Anal. Chem. **60**, 269 (1988).
[3]V. Y. Young, G. B. Hoflund, and A. C. Miller, Surf. Sci. **235**, 60 (1990).
[4]O. Melendez, G. B. Hoflund, R. E. Gilbert, and V. Y. Young, Surf. Sci. **251-252**, 228 (1991).
[5]A. C. Miller, in *Treatise on Analytical Chemistry,* 2nd ed., edited by J. D. Winefordner (Wiley, New York, 1989), Vol. 11, Part 1, Chap. 5, p. 253.
[6]M. Hou, Vacuum **39**, 309 (1989).
[7]Y. Xia, X. Xu, C. Tan, L. Mei, H. Yang, and X. Sun, J. Appl. Phys **69**, 439 (1991).
[8]E. Taglauer and W. Heiland, Appl. Phys. **9**, 261 (1976).
[9]A. A. Abrahamson, Phys. Rev. **178**, 76 (1969).
[10]A. A. Abrahamson, R. D. Hatcher, and G. H. Vineyard, Phys. Rev. **121**, 159 (1961).
[11]O. B. Frisov, Zh. Eksp. Teor. Fiz. **33**, 696 (1958) [Sov. Phys. JETP **6**, 534 (1958)].
[12]G. Moliere, Z. Naturforsch. **2a**, 133 (1947).
[13]E. Everhart, G. Stone, and R. J. Carbone, Phys. Rev. **99**, 1287 (1955).
[14]E. A. Parilis, in *Proceedings of the Seventh International Conference on Phenomena in Ionized Gases,* edited by R. Perovic and D. Tosic (Gradevinska Knjiga, Beograd, 1966), Vol. 1, p. 129.
[15]J. F. Ziegler, J. P. Biersack, and W. Littmark, *Stopping and Range of Ions in Solids* (Pergamon, New York, 1985), Chap. 2.
[16]A. Benninghoven, F. G. Rudenauer, and H. W. Werner, *Secondary Ion Mass Spectrometry: Basic Concepts, Instrumental Aspects, Applications and Trends* (Wiley, New York, 1987), p. 16.
[17]R. E. Gilbert, D. F. Cox, and G. B. Hoflund, Rev. Sci. Instrum. **53**, 1281 (1982).